Supplemental Material for "Direct visualization of surface spin-flip transition in $MnBi_4Te_7$"

Wenbo Ge[1], Jinwoong Kim[1], Ying-Ting Chan[1], David Vanderbilt[1], Jiaqiang Yan[2], and Weida Wu[1]*.

[1]*Department of Physics and Astronomy, Rutgers University, Piscataway, NJ 08854, USA.*

[2]*Materials Science and Technology Division, Oak Ridge National Laboratory, Oak Ridge, Tennessee 37831, USA.*

*Correspondence to: wdwu@physics.rutgers.edu (WW).

Methods

Sample preparation. Platelike single crystals of $MnBi_4Te_7$ were grown out of a Bi-Te flux and have been well characterized by measuring the magnetic and transport properties. Crystals used in this study order magnetically below $T_N = 13\,\mathrm{K}$ with ferromagnetic Mn-Te layers coupled antiferromagnetically. At 2 K, $MnBi_4Te_7$ shows a spin-flip transition at H_{SF} = 0.2 T with a magnetic field applied along the crystallographic c-axis.

MFM measurement. The magnetic imaging was carried out in a homemade cryogenic magnetic force microscope (MFM) interfaced with a commercial phase-lock loop and SPM Controller (SPECS). MFM tips were prepared by depositing nominally 150 nm Co film onto bare tips of piezoresistive cantilevers (spring constant $k \approx 3$ N/m, resonant frequency $f_0 \approx 42$ kHz) using sputtering. MFM measurements were performed in a constant height mode with nominal lift height ~100 nm above the sample surface. The change of cantilever resonant frequency (MFM signal) is proportional to out-of-plane stray field gradient. The tip-surface contact potential difference was balanced to minimize electrostatic interaction. Bright (dark) MFM contrast represents repulsive (attractive) interaction, where magnetizations are anti-parallel (parallel) with the external field.

Simulation. Our previous simulation predicted that spin-flop states do not occur in the high-anisotropy limit, regardless of whether the revised or original Mill's model is used[1]. Spin-flip states are easier to treat theoretically, as optimal spin-canting angles do not have to be computed. We directly evaluate the energies of a discrete set of candidate collinear spin configurations and determine the minimum-energy configuration as a function of the external field and the parameters describing the surface spin Hamiltonian.

1. Topography of the cleaved surface in full scanning range

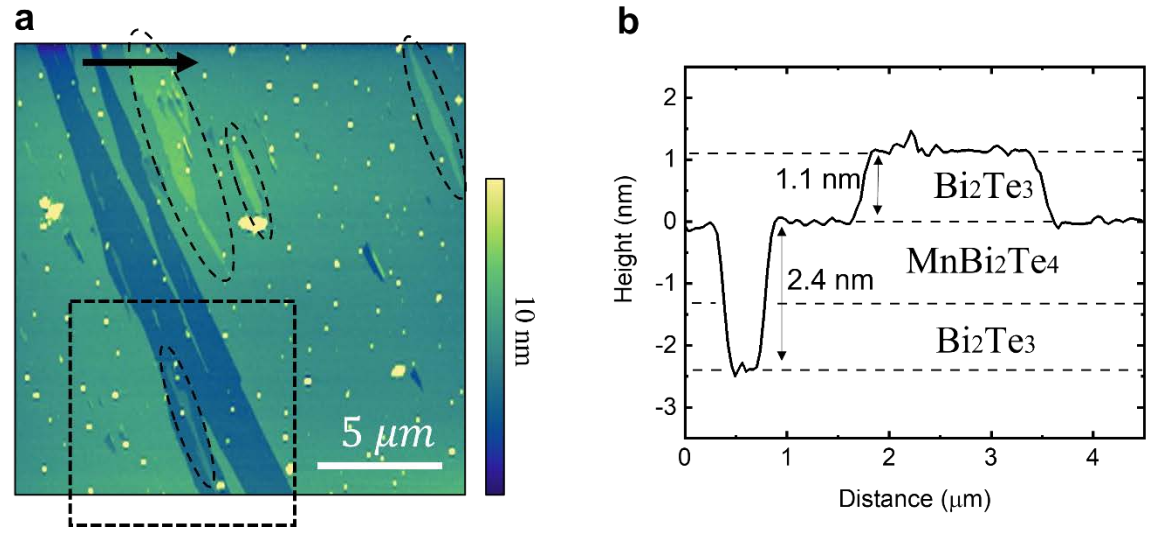

Fig. S1 | Topographical image of the cleaved surface taken at 5.5 K with a line profile along the arrow. In **a**, the area inside the box corresponds to the scanning area of FIG. 1. in the main text. The circled islands correspond to Bi_2Te_3. The scan size of the image is 18 μm by 18 μm. The Scale of the image is 10 nm as labeled.

Fig. S1**a** shows the topography of the cleaved surface. The small displacement of the scanning area inside the box is caused by the hysteresis of MFM walker. Unless specified, this topographical image corresponds to all the MFM images that appear in the main text and the supplemental material. A topographical line profile along the arrow is shown in Fig. S1**b**. The depth of the trench (~2.4nm) agrees with that in FIG. 1. of the main text. On the terrace above the trench, there is also an island of height 1.1 nm suggesting it is Bi_2Te_3. This topographical image with its line profile further confirms the termination of the cleaved surface in our scanning range is dominated by $MnBi_2Te_4$. There are only a few Bi_2Te_3 islands, which are highlighted by dashed ellipses. Note that any step contains a $MnBi_2Te_4$ layer could cause MFM contrast because a single $MnBi_2Te_4$ layer is ferromagnetically ordered. The domain walls can be distinguished from the topographical steps in the MFM images once the topography of the scanned area is known.

2. Bulk spin-flip transition in $MnBi_4Te_7$

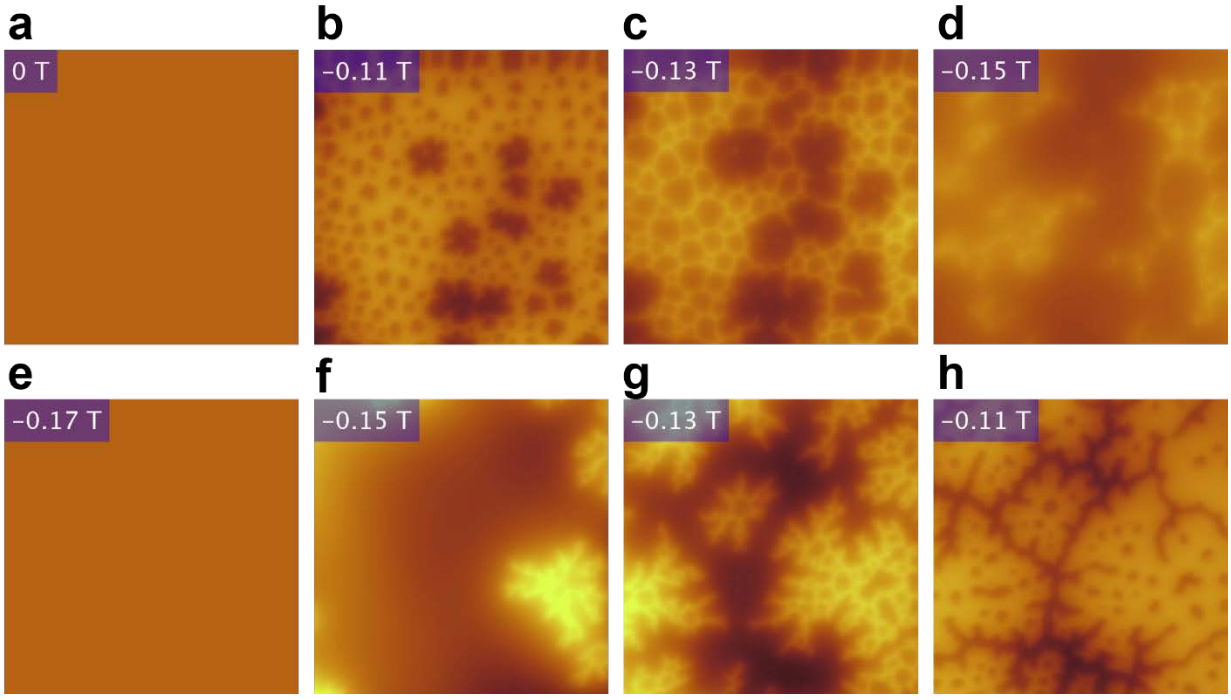

Fig. S2 | MFM images of bulk spin-flip transition at 5.5 K. a-e, MFM images taken while the external field is increased from 0 T to -0.17 T, where the sample is saturated. Negative sign indicates the external field points down. **f-h**, MFM images taken while the external field is decreased. The color scale for the MFM images is 20 Hz.

Fig. S2 shows the MFM images of bulk spin-flip transition, which occurs between 0.1 T and 0.17 T. Fig. S2**a** is the MFM image taken after zero field cooling. Bulk ferromagnetic domain does not appear at zero field until the external field reaches −0.1 T. Fig. S2**b-d** capture the development of bulk spin-flip transition. Bubble-like FM domains nucleate and expand as the field is increased. Until −0.17 T, the whole scanning area is occupied by a single FM domain indicating the sample is saturated (Fig. S2**e**). Fig. S2**f-h** shows the recovery of AFM domains as the field is decreased. The grown of dendritic AFM domains is clearly visible from the MFM images. The MFM images of bulk spin-flip transition are further binarized such that pixels in dark FM domains are assigned to 0 and pixels in bright AFM domains are assigned to 1. The FM domain portion in FIG. 2**i** of the main text is then calculated from the binarized image[2]. $\mu_o H_{BSF} \approx 0.13$ T is determined by the middle point of BSF transition where the FM domain portion equals 0.5. Note that, the typical MFM signal of bulk spin-flip transition (~15 Hz) is several hundred times larger than that of AFM domains (~20 mHz). As a result, any MFM contrast caused by surface layers is no longer visible in this scale.

3. Configuration of AFM domain wall

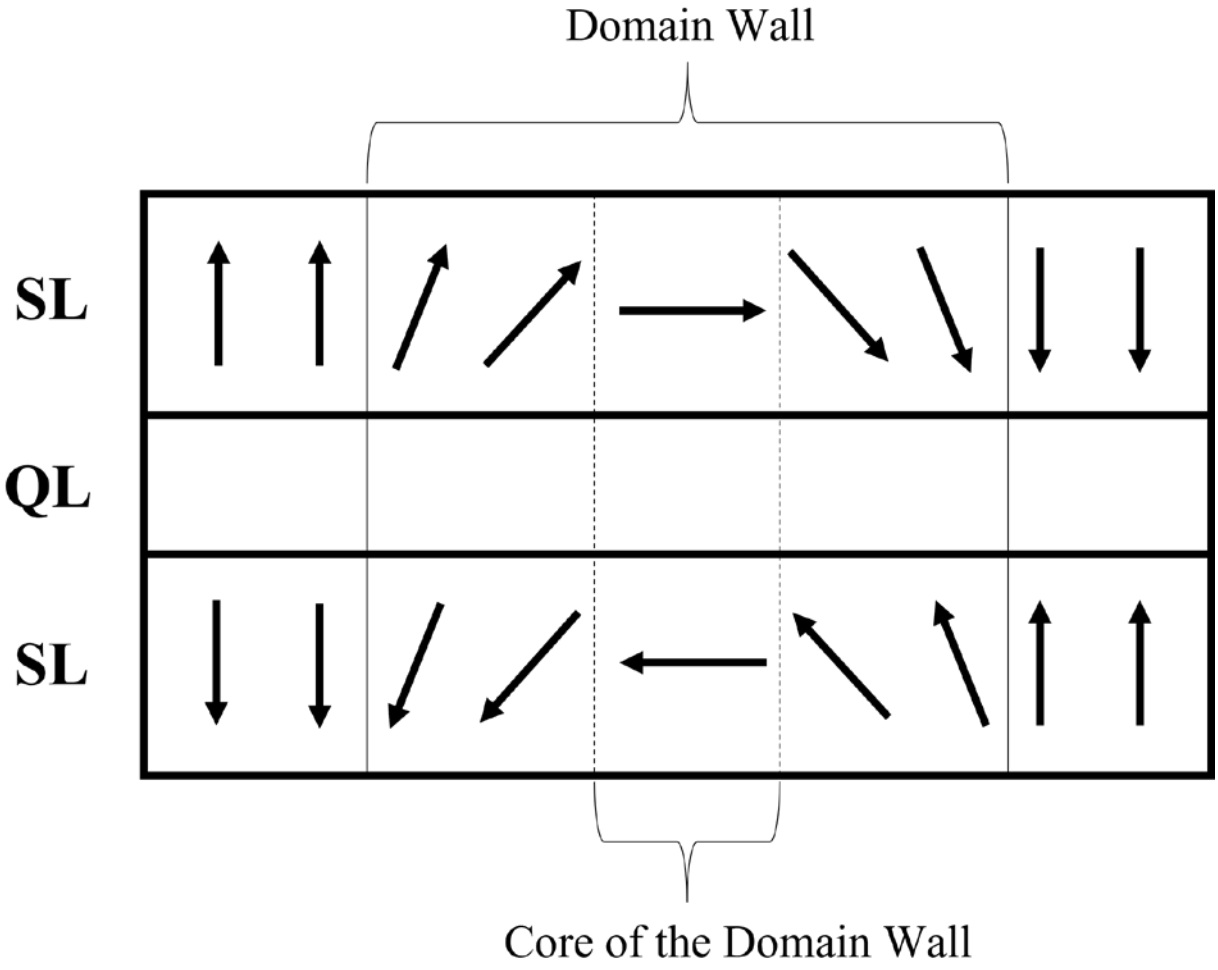

Fig. S3 | Schematics of the spin configuration inside the domain wall of $MnBi_4Te_7$ at 0 T.

A schematic diagram is shown in Fig. S3 to illustrate the domain wall configuration, which is omitted in FIG. 1. (e). Due to the competition between the strong intra-plane exchange coupling and the uniaxial anisotropy, the magnetic moment inside the domain wall should smoothly rotate from up to down or vice versa across the domain wall. Note that, MFM cannot distinguish between Bloch type and Neel type domain wall. Here, we plot a Neel type domain wall only for easy illustration of the winding of magnetic moments.

4. AFM domain walls induced by field cooling

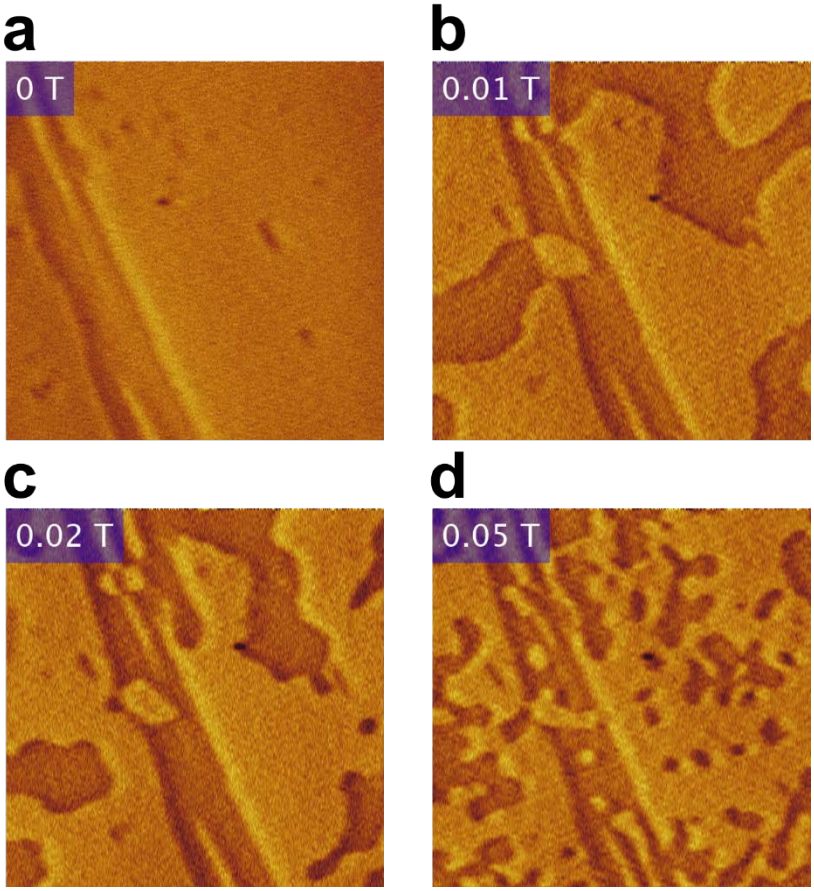

Fig. S4 | MFM images at 5.5 K in zero field after different field cooling. The cooling field is labeled at the corner in each image. The color scale is 50 mHz.

Fig. S4 shows the MFM images taken after cooling the sample from above T_N under different magnetic field. Domain wall does not appear in the scanning area after zero field cooling, which suggests the sample has few nucleation sites (Fig. S4**a**). In other words, the sample quality is very good. Domain walls appears after cooling the sample under finite magnetic field. As shown in Fig. S4**b-d** domain wall density increases with the cooling field. This is because higher domain wall density gains Zeeman energy[3].

5. Complete MFM data of SSF transition

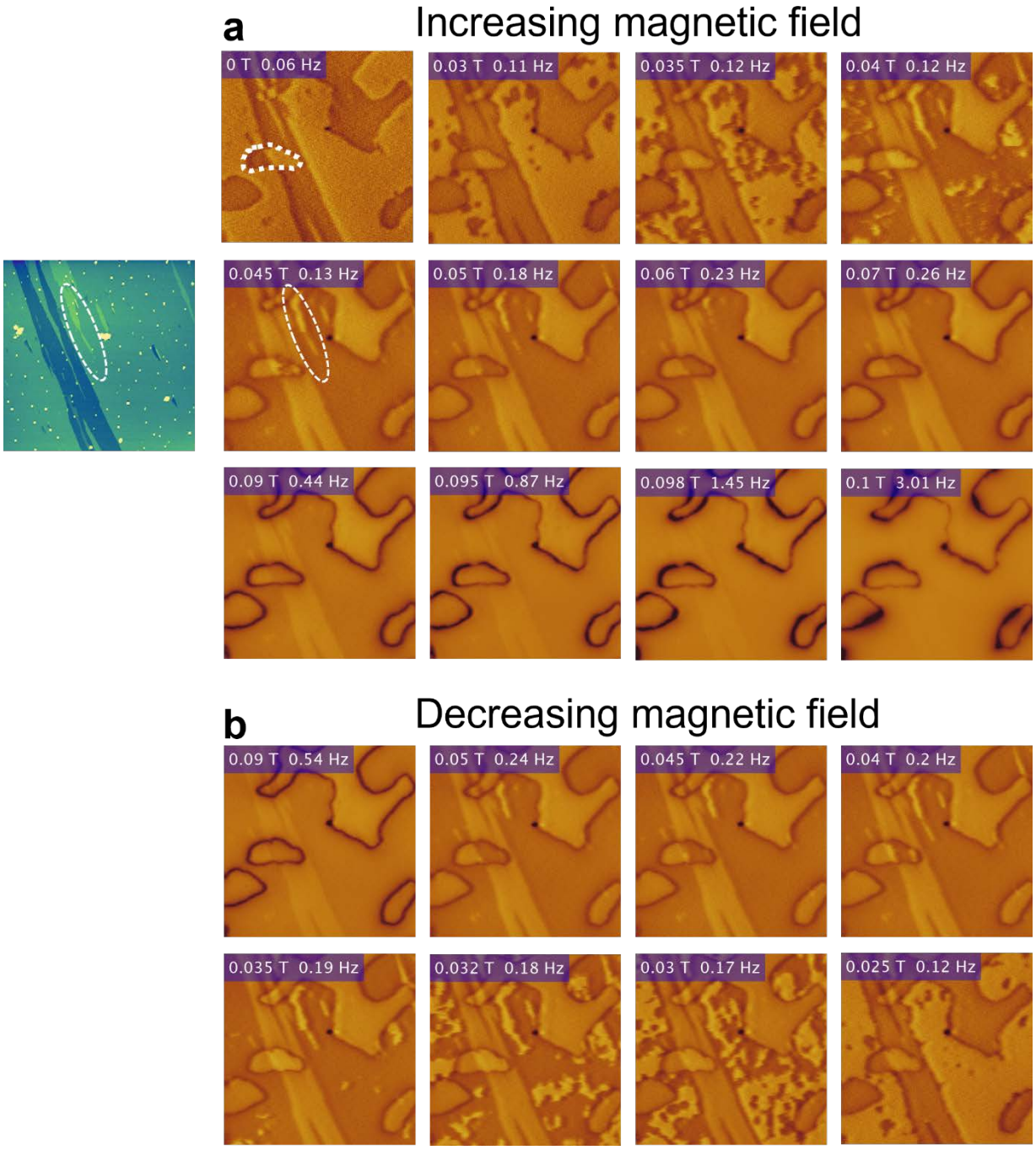

Fig. S5 | A complete data set of MFM images at 5.5 K in various magnetic fields showing SSF transition. a. MFM images taken with increasing magnetic field. The topographical image is placed on the side. **b**. MFM images taken with decreasing magnetic field. The corresponding magnetic field and color scale are labeled at the corner.

A complete set of MFM images showing SSF transition is shown in Fig. S5. In addition to the SSF transition on β domain discussed in the main text, more details can be found here. First, notice the

small domain highlighted in the zero-field image in **a**. The domain is cut in the middle by a SL+QL step. Consequently, half of this domain has antiparallel surface. It also undergoes SSF transition as shown in Fig. S5**a** (MFM image taken at 0.045 T). Interestingly, the SSF transition field in the trench (~0.045 T) is higher than that in the β domain (~0.035 T). This is because the surface layer in the trench has more neighboring layers to be coupled with. Therefore, the SSF transition in the trench occurs at higher field. Moreover, even though the cleaved surface is dominated by $MnBi_2Te_4$ layer termination, there are some islands of Bi_2Te_3 layer on the surface as discussed in Fig. S1. As shown in the MFM image taken at 0.045 T in **a**, the area terminated in quintuple layer is marked by a dashed ellipse. This area belongs to β domain, however, the SSF transition in this area is evidently delayed to higher field (~0.06 T). This is possibly due to the Bi_2Te_3 island on the surface enhances the coupling between the under covered $MnBi_2Te_4$ layer and the bulk via RKKY interaction.

6. MFM images of SSF transition in negative field.

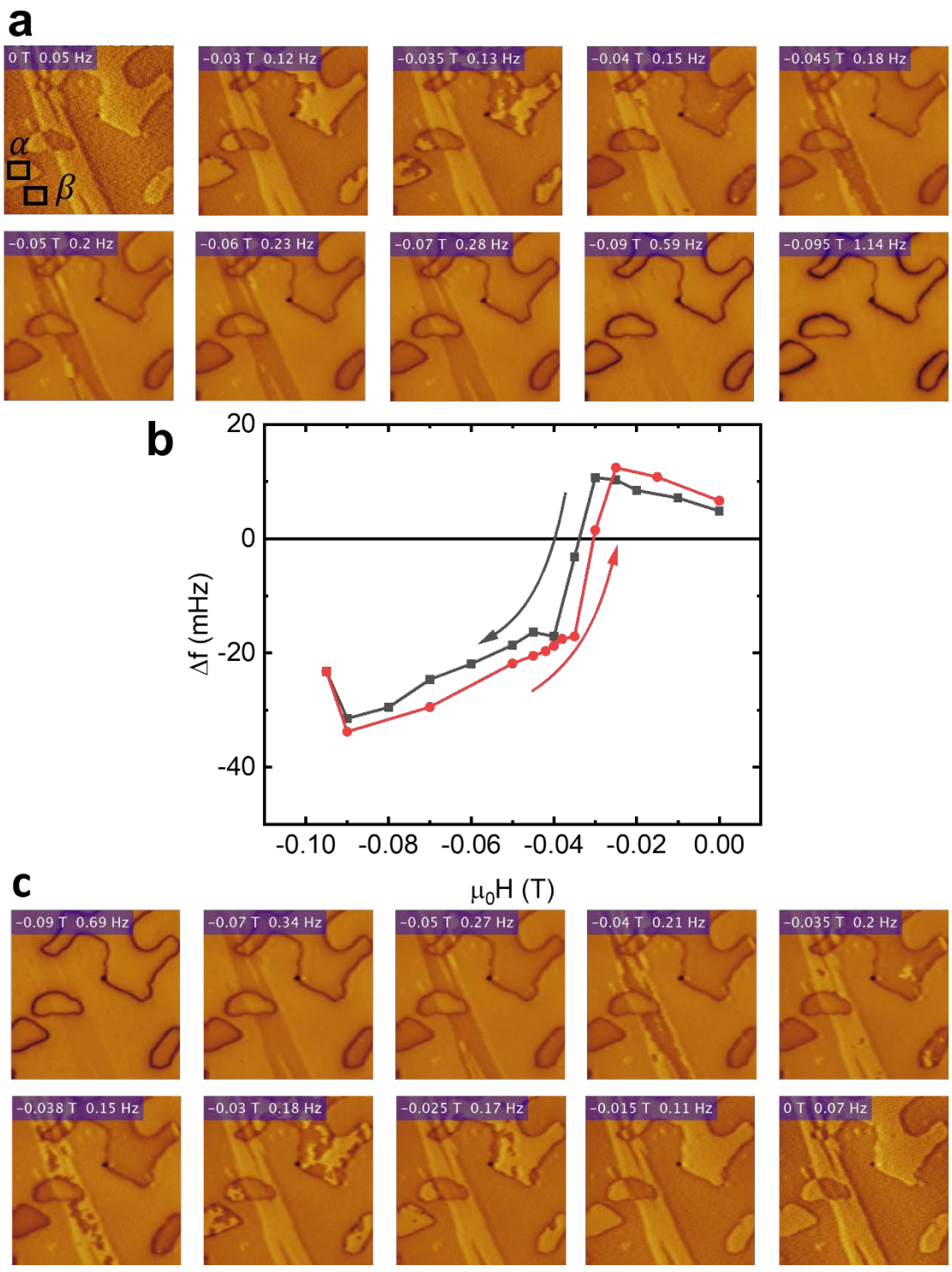

Fig. S6 | MFM images of SSF transition at negative field. a, c. MFM images taken with increasing and decreasing field, respectively. **b.** MFM signal contrast between α and β domain as labeled in **a**.

Surface spin-flip transition is also seen from the MFM images taken at negative field (field direction pointing down). The domain process and the transition field are similar to that at positive field. In Fig. S6**a** and **c**, partially flipped domain α is clearly visible. The MFM signal difference between α and β in Fig. S6**b** shows similar behavior as FIG. 2. (i) in the main text.

7. Phase diagram of $MnBi_4Te_7$

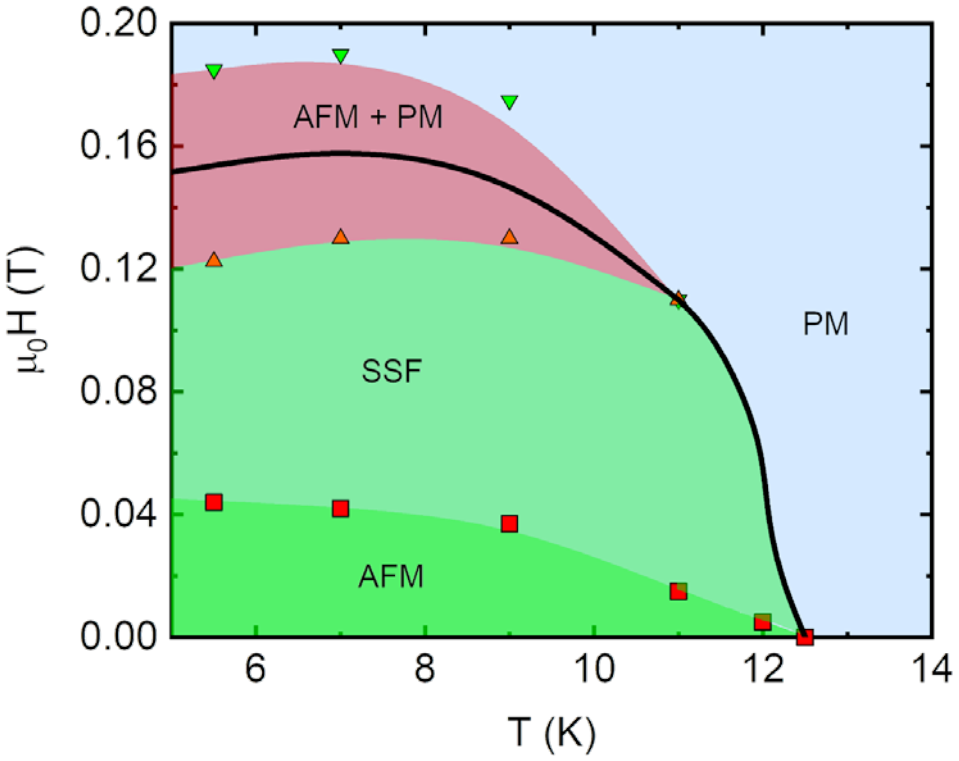

T (K)	H_{SSF}/H_{BSF}
5.5	0.286
7	0.262
9	0.243
11	0.136

Fig. S7 | Phase diagram of $MnBi_4Te_7$ derived from the transport measurement of $MnBi_4Te_7$ (black solid line) in combined with MFM imaging (colored dots) on a different $MnBi_4Te_7$ sample. The Neel temperature of $MnBi_4Te_7$ is 12.5 K for the sample. Below T_N, red square dots label the SSF transition boundary. The width of this boundary is smaller than 0.05 T based on MFM imaging. The black solid line is the BSF transition boundary, which has noticeable width as indicated by the pink region. The ratio between SSF and BSF transition is summarized in the table below the phase diagram. Below 11 K, the SSF transition field is approximately 1/4 of the bulk one, which agrees well with the sample discussed in the main text.

8. Absence of SLSF transition when $\lambda_J \lambda_s > 1$

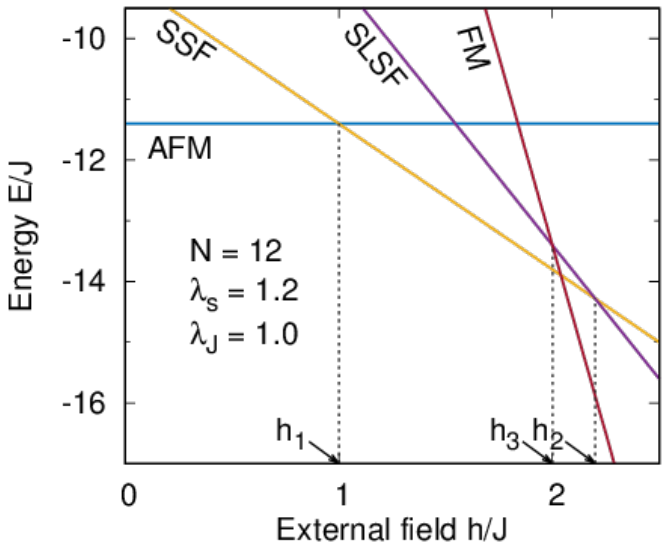

Fig. S8 | Total energy as a function of exchange field, for the four magnetic phases with twelve spin-lattice sites (N = 12) and enhanced surface spin moment (λ_s = 1.2).

As shown in Fig. S8, sequential phase transitions: AFM to SSF to FM phase are expected with increasing external field. The SLSF phase disappears due to enhanced surface parameters ($\lambda_J \lambda_s > 1$).

9. Partial second layer spin-flip transition induced by field “annealing” experiment

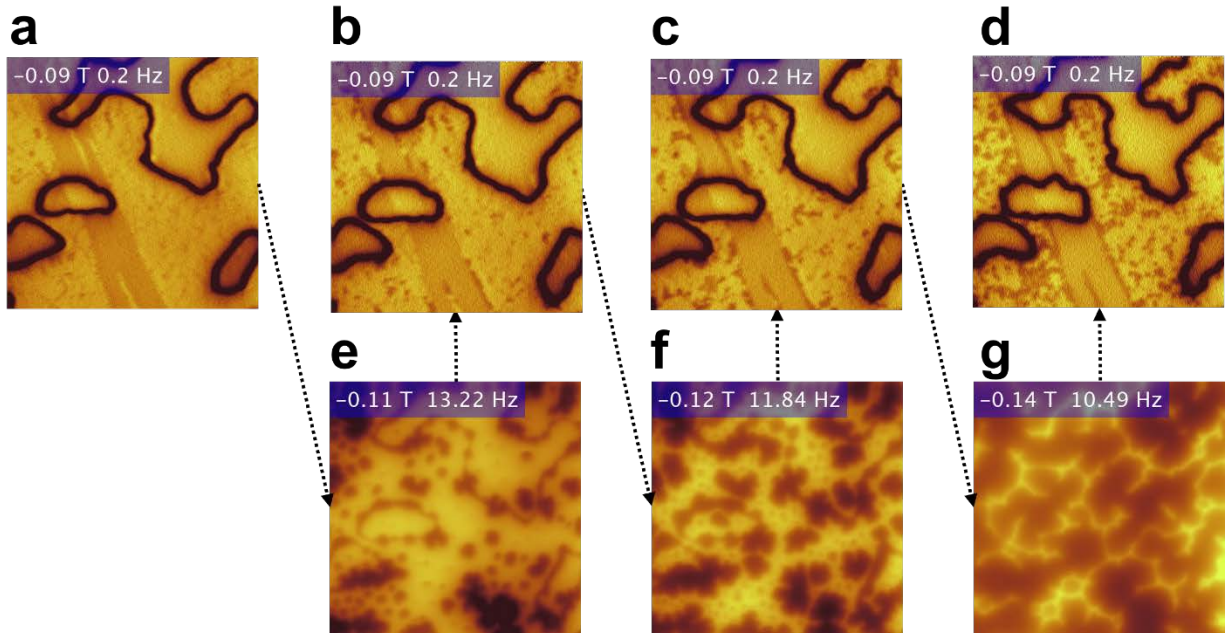

Fig. S9 | MFM images of SLSF transition measured at 5.5 K. a, MFM image taken with a −0.09 T external field after sweeping magnetic field to −0.1 T, which is the onset of BSF transition. **b, c, d**, MFM data taken while the external field was reduced to −0.09 T and the sample returns to antiferromagnetic state from the bulk spin-flip transition. **e, f, g**, MFM images taken at −0.11T, −0.12T and −0.14T respectively. The sample was undergoing BSF transition at these fields. The black arrows indicate the sequence of MFM images. The gradually nucleating and growing domains in **b, c** and **d** is the signature of SLSF transition.

10. MFM sensitivity limit for few-layer flakes

In FIG. 1. of the main text, domain contrast can be seen across a SL+QL step (red arrow). This contrast is purely caused by the extra ferromagnetic SL on the step, indicating our MFM measurement can resolve the signal from a single-layer $MnBi_2Te_4$. In atomically thin samples with odd number of layers, the stray field from the extra layer is uncompensated and the overall contribution is equivalent to that of a single-layer $MnBi_2Te_4$. Therefore, our MFM should be able to resolve the domain contrast of thin films with odd number of layers. However, the cancelation of stray field in thin flakes with even number of layers ($N<10$) is almost perfect, leading to a significantly smaller signal, which might be smaller than the sensitivity limit of our MFM system.

References and Notes:

1. P. M. Sass, *et al.* Robust A-Type Order and Spin-Flop Transition on the Surface of the Antiferromagnetic Topological Insulator $MnBi_2Te_4$. *Phys. Rev. Lett.* **125**, 037201 (2020).
2. Ge, W. *et al*. Direct evidence of ferromagnetism in $MnSb_2Te_4$. *Phys. Rev. B* **103**, 134403 (2021).
3. Sass, P. M. *et al.* Magnetic Imaging of Domain Walls in the Antiferromagnetic Topological Insulator $MnBi_2Te_4$. *Nano Lett.* **20**, 2609–2614 (2020).